



Relative dispersion of clustered drifters in a small micro-tidal estuary



Kabir Suara^{a,*}, Hubert Chanson^b, Michael Borgas^c, Richard J. Brown^a

^a Queensland University of Technology (QUT), Australia

^b School of Civil Engineering, The University of Queensland, Australia

^c Marine and Atmospheric Research, Commonwealth Scientific and Industrial Research Organisation (CSIRO), Australia

ARTICLE INFO

Article history:

Received 31 October 2016

Received in revised form

23 March 2017

Accepted 3 May 2017

Available online 6 May 2017

ABSTRACT

Small tide-dominated estuaries are affected by large scale flow structures which combine with the underlying bed generated smaller scale turbulence to significantly increase the magnitude of horizontal diffusivity. Field estimates of horizontal diffusivity and its associated scales are however rare due to limitations in instrumentation. Data from multiple deployments of low and high resolution clusters of GPS-drifters are used to examine the dynamics of a surface flow in a small micro-tidal estuary through relative dispersion analyses. During the field study, cluster diffusivity, which combines both large- and small-scale processes ranged between, 0.01 and 3.01 m²/s for spreading clusters and, −0.06 and −4.2 m²/s for contracting clusters. Pair-particle dispersion, D_p^2 , was scale dependent and grew as $D_p^2 \sim t^{1.83}$ in streamwise and $D_p^2 \sim t^{0.8}$ in cross-stream directions. At small separation scale, pair-particle ($d < 0.5$ m) relative diffusivity followed the Richardson's 4/3 power law and became weaker as separation scale increases. Pair-particle diffusivity was described as $K_p \sim d^{1.01}$ and $K_p \sim d^{0.85}$ in the streamwise and cross-stream directions, respectively for separation scales ranging from 0.1 to 10 m. Two methods were used to identify the mechanism responsible for dispersion within the channel. The results clearly revealed the importance of strain fields (stretching and shearing) in the spreading of particles within a small micro-tidal channel. The work provided input for modelling dispersion of passive particle in shallow micro-tidal estuaries where these were not previously experimentally studied.

© 2017 Elsevier Ltd. All rights reserved.

1. Introduction

In estuaries and natural water channels, the estimation of diffusivity is important for the modelling of scalar transport and mixing. It allows modeller to effectively predict the transport of scalars for water quality monitoring (e.g. salinity distribution and chlorophyll level), pollution run-off tracking (e.g. waste water and accidental spillage) and ecosystem monitoring (e.g. larvae and algae transport). Many applications can be formulated in a Lagrangian framework (Haza et al., 2008). The dispersion effect of an Eulerian velocity field on particle-laden turbulent flow can be parameterised by 'eddy' absolute and relative diffusivities (Taylor, 1921; Richardson, 1926; LaCasce and Bower, 2000). Absolute dispersion (and associated diffusivity) is equivalent to variance of the ensemble average of distances covered by large numbers of particles released from a common starting point. Relative

dispersion (and associated diffusivity) characterises the distortion of clusters of particles, relative to a reference frame, fixed to the centre of mass of the cluster. Relative dispersion is more closely related to mixing of scalars and forms the focus of the present study (Sawford, 2001; Haza et al., 2008).

Relative dispersion in a fluid is a fundamental property, study of which that dates back to Richardson (1926). An extensive review of the analytical and statistical frameworks is well compiled in the literature (Sawford, 2001; LaCasce, 2008; Salazar and Collins, 2008). Richardson's power law relationship for relative dispersion, D , to elapsed time, t , $D^2 \sim \epsilon t^\alpha$ with $\alpha = 3$ and relative diffusivity, K , $K_p \sim d^\gamma$ with $\gamma = 4/3$ are found to be related to the Kolmogorov's energy cascade law $E(k) \sim \epsilon^{2/3} k^{-5/3}$, where ϵ is the turbulence kinetic energy (TKE) dissipation rate, d is the length scale and k is the wave number, in 3D homogeneous flow in isotropic turbulence within the inertial range (Kolmogorov, 1941; Batchelor, 1952). Many environmental flows are quasi two dimensional, dominated by inhomogeneity and anisotropy, which raise the question of the applicability of such relationships. Richardson-like relationships have been observed in the subsurface flow in the Gulf of Mexico,

* Corresponding author. Science and Engineering Faculty, Queensland University of Technology, 2 George St., Brisbane QLD 4000, Australia.

E-mail address: k.suara@qut.edu.au (K. Suara).

with a power $\gamma = 2.2$ at time, $t > 10$ days and length scale, $l > 50$ km (LaCasce and Ohlmann, 2003). Brown et al. (2009) observed a power law relationship with $\gamma = 4/3$ and $\alpha = 1/5$ with time, $t \leq 100$ s and length scale range of 1–10 m in a rip channel with the dispersion dominated by horizontal shear. In addition, different spatial scales may have radically different laws for relative dispersion as demonstrated by observations in a large estuary (Soomere et al., 2011). The range of these observations indicates a deviation from existing theory due to the combination of underlying physical processes and experimental constraints. Quantifying and understanding the behaviour of clustered particles provide guidance for modelling dispersion of instantaneous release of material (e.g. pollutants and waste discharges) and concentration fluctuation in dispersive plume in such system. Interestingly, no other literature to date has experimentally examined relative dispersion of passive particles in shallow micro-tidal estuaries.

Until recently, turbulent mixing in tidal-dominated shallow estuaries has been studied using Eulerian acoustic devices and dye-tracer experiments (Kawanisi, 2004; Situ and Brown, 2013). Limitations in position accuracy, cost and size have restricted the use of GPS-tracked drifters to large water bodies. Drifters have been used to study the underlying fluid dynamics and scalar particle dispersion at various scales in oceans (Poje et al., 2014), seas (Schroeder et al., 2012), lakes (Stocker and Imberger, 2003), large estuaries (Tseng, 2002), nearshore (Brown et al., 2009) and recently tidal inlets (Whilden et al., 2014; Spydell et al., 2015). While these previous studies focussed on the relatively large-scale processes defined by the domain size and spatio-temporal resolution of available instruments, small-scale processes ($O(100$ s) and $O(\text{few metres})$) have rarely been studied. Recent improvements in GPS technology have paved the way for the development of high resolution (HR) Lagrangian drifters to study dispersion in shallow waters (with depth $\sim O(\text{few metres})$), where processes of interest occur in small scales ($O(100$ s) and $O(\text{few metres})$) (Suara et al., 2015b).

This research studies the spatio-temporal variation of velocity and dispersion in typical shallow water estuaries to underpin the current modelling efforts in shallow waters. This paper presents a new datasets and analysis of clustered HR and low resolution (LR) drifters, deployed repeatedly within a section of a micro-tidal estuary at different tidal phases. The present effort: (i) examines the turbulence characteristics of the surface flow, (ii) seeks Richardson-like power relationships for the pair-particle separation against time and the diffusivity against length scale of separation, and (iii) identifies the dominant mechanisms responsible for dispersion using cluster analysis.

2. Materials and method

2.1. Field observations

Drifter deployments were performed in three separate experiments, alongside fixed instruments, during a 48-h field study at Erapah Creek. Erapah Creek is a shallow tidal estuary, which discharges into Moreton Bay, Eastern Australia. This field site serves as nature's laboratory due to its small size and low level of recreational activities that could interfere with experiments. The field has been extensively used to study the turbulence characteristics of small tidal estuaries (Trevethan and Chanson, 2009; Chanson et al., 2012). The estuarine zone extends to 3.8 km inland and is well sheltered from wind by mangroves. The channel exhibits irregular boundaries, which may cause a high degree of variability in the cross-stream flow at different cross sections (Fig. 1). Fig. 1 shows the line map of the field and the cross sections close to the experimental test section. The channel widens at the channel mouth. The

maximum depth along the test section was about 2.5 m below Mean Sea level (MSL). The channel width was limited to about 60 m at high tide and 25 m at low tide. Drifter deployments were made at flood and slack tides within the straight test section between adopted middle thread distance (AMTD) 1.60 and 2.05 km measured from the mouth, i.e. between cross section Y and Z (Fig. 1).

The HR drifters, equipped with differential RTK-GPS integrated receiver and sampled at 10 Hz with position accuracy ~ 2 cm, were designed and constructed by the Queensland University of Technology and are described in Suara et al. (2015b). The LR drifters contained off-the-shelf Holux GPS data loggers with absolute position accuracy, between 2 and 3 m, and were sampled at 1 Hz. The HR drifters were 19 cm in diameter and 26 cm in length while the LR drifters were 4 cm in diameter, 50 cm and 25 cm in length for the long and short versions¹, respectively. The drifters were positively buoyant for continuous satellite position fixation with unsubmerged height < 3 cm in order to limit the direct wind effect. The resulting direct wind slip, estimated as less than 1% of the ambient wind, is not accounted for in the analysis. The set of drifters, used in this study, had velocities that compare well with Acoustic Doppler Current Profilers (ADCP) surface horizontal velocity measurements (squared-correlation coefficient $R^2 > 0.9$). Drifters were released in clusters of four to five near the centre of the channel. Five clusters of drifter with cluster IDs¹ HR, LRC1, LRC2, LRC3 and LRC4 were used. Note that the drifter deployments are identified by experiment, deployment, and cluster ID. For example E1 is experiment 1, D1 is deployment 1 and HR is high resolution. For each deployment, clusters were formed in quadri/pentagonal pattern spaced ~ 1 m between drifters, while a time window of ~ 3 min was maintained between cluster deployments. The flood deployments were made at AMTD 1.6 km and allowed to drift until they reached the end of the test section at AMTD 2.05 km before collection for re-deployment. The slack water deployments were made within 100 m of the ADV deployed in cross section U (Fig. 1).

2.2. Environmental conditions and drifter deployments

Table 1 below summarises the environmental conditions during individual drifter experiments. A range of tide, wind and flow conditions were encountered during the 48-h field study and they are presented in Supplementary Fig. S1. The average tidal range was 2.03 m. Erapah Creek is characterised by a diurnal wind pattern. Because the channel was reasonably sheltered by mangroves, the average day wind speed between 0 and 4 m/s were mostly aligned with the streamwise direction while the night wind speed varied between 0 and 1 m/s without a directional preference.

2.3. Data quality control

The drifter datasets were quality controlled by removal of spurious data points and sections of the tracks where they were evidently trapped in the banks, obstructed or interrupted based on the experimental event log. Spurious position data were identified as those with velocity and acceleration greater than some specified thresholds. The choice of the threshold was subject to the nature of the flow. The maximum tidal flow velocity in Erapah Creek was about 0.3 m/s, thus a threshold was defined as twice this velocity and an acceleration threshold of 1.5 m/s² was also defined, in accordance with previous experimental studies (Trevethan et al.,

¹ HR = 4 HR drifters; LRC1 = 5 LR drifters (long version); LRC2 = 4 LR drifters (long version); LRC3 = 5 LR drifters (short version); LRC4 = 4 LR drifters (short version).

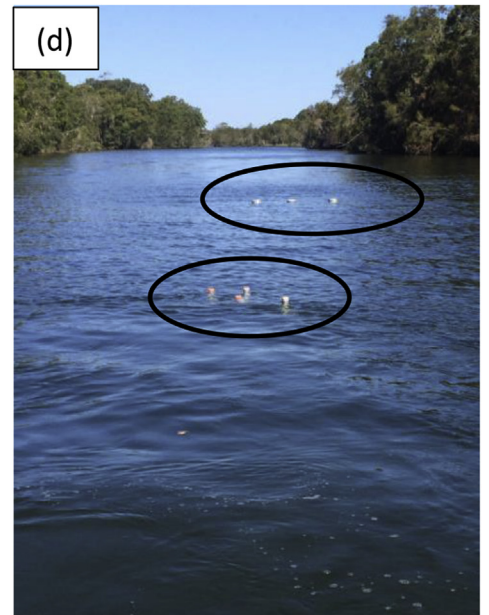
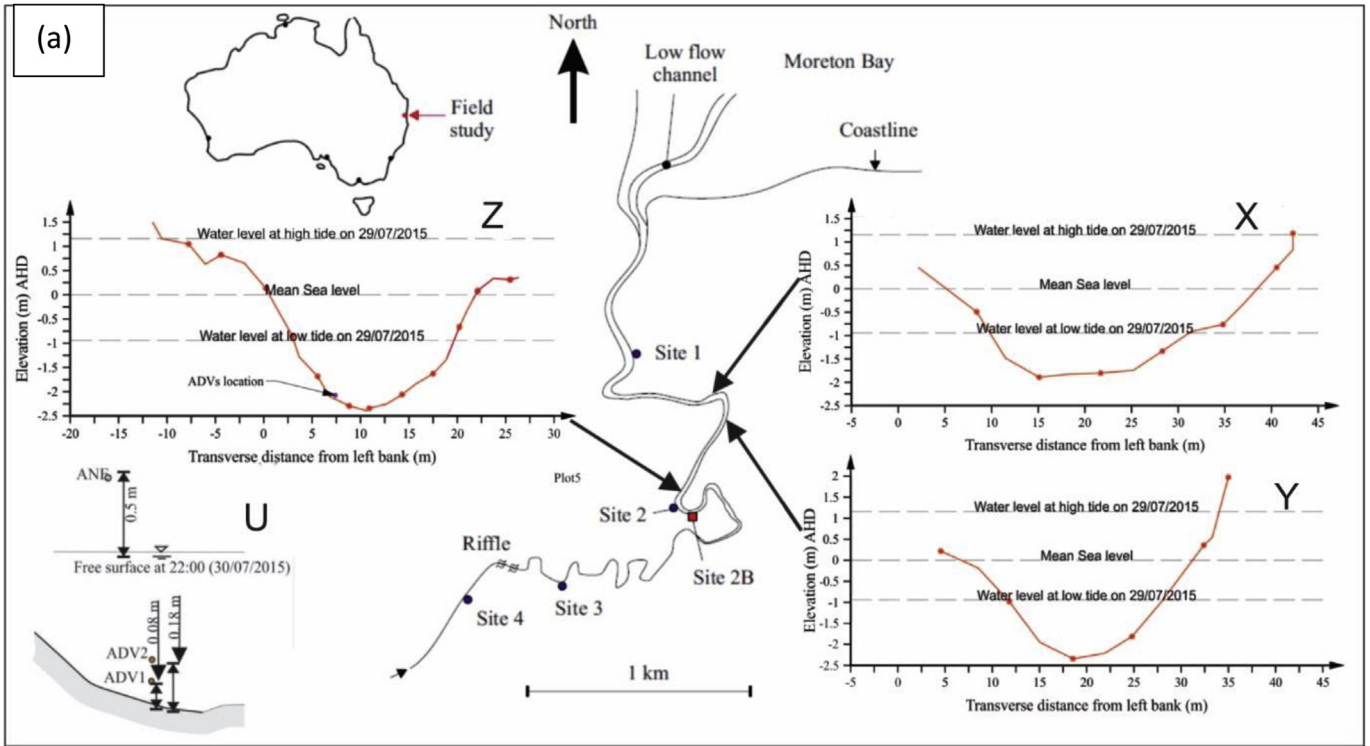


Fig. 1. (a) Epraph Creek estuarine zone, including surveyed cross sections (X–Z) on 30 July 2015; ADVs, ADCP and a Sonic anemometer (ANE) were deployed downstream cross section Z as arranged in U; (b) Aerial view of Epraph Creek showing the experimental test section in red rectangle (Nearmap, 2015); (c) Photograph of high and low resolution drifters; (d) Photograph of clusters of HR and LR drifters (black ellipse) about 2 min after deployment; upstream of cross section Y.

2008; Suara et al., 2015a). Flagged data were then replaced with linearly interpolated points using data at two valid end points where the gap was less than 20 s. Gaps greater than 20 s were considered omitted and were not replaced. The drifter data were transformed to channel-based streamwise (s), cross stream (n), up (u) coordinate system based coordinate following (Legleiter and Kyriakidis, 2006; Suara et al., 2015b). Streamwise locations s , are AMTD of the channel centreline measured upstream from the channel mouth while cross streams, n are positive from channel

centreline to the left downstream. For the HR drifters, the position time series was further treated with a low-pass filter of cut-off frequency, $F_c = 1$ Hz and subsampled to intervals of 1 s to remove the instrument noise at high frequencies (Suara et al., 2015b). The velocities were obtained by central differencing of the quality controlled position time series. The position time series of the LR drifter contained some large uncertainty at frequencies greater than 0.1 Hz, which impaired the direction estimates, particularly during low flow speed. Therefore, to estimate the ‘true’ (average)

Table 1
Overview of the environmental conditions of the field and durations of each experiment; Wind data collected from a two dimensional sonic anemometer deployed about 1 m from the water surface. Wind direction measured clockwise from positive streamwise direction, downstream; Water surface horizontal velocity magnitude, V_H measured from the ADCP as average of the valid upper 0.2 m after quality control.

Experiment	Tidal type	Tidal range (m)	Wind speed range (m/s)	Average wind speed (m/s)	Average wind dir. (deg.)	Average water surface V_H (m/s)	Deployment number	Average duration (s)
E1	Flood	1.75	0–1.76	0.31	137	0.48	D1	1589
							D2	1777
							D3	2509
E2	Flood	2.25	0–4.43	0.65	10	0.57	D1	693
							D2	1977
							D3	2560
E3	Slack	1.70	0–3.05	0.59	70	0.19	D1	2030
							D2	2020

flow direction, the LR drifter position time series were low-pass filtered with $F_c = 0.05$ Hz. The velocities were then obtained by combining low-pass filtered position time series with the de-spiked speed time series, Sp , such that:

$$V_s(t) = Sp(t) \times \sin \theta(t), \quad V_n(t) = Sp(t) \times \cos \theta(t) \quad \text{and} \quad \theta(t) = \arctan\left(\frac{s(t)}{n(t)}\right), \quad (1)$$

where V_s and V_n are the streamwise and cross-stream velocities, respectively, while θ is the direction based on the position time series (s , n).

2.4. Drifter tracks and basic flow observations

Fig. 2 shows the spaghetti plot of all drifter tracks for the three different experiments, E1, E2 and E3. In general, drifter trajectories were within a 15 m span of the channel centreline. The tracks followed the meandering of the channel in response to the variable cross-stream velocity. The cross-stream flow velocity variations were mainly influenced by the combination of wind-induced currents on the subsurface layer, irregular bathymetry and reflection of the tidal forcing against meandering boundaries resulting in internal resonance, which is the sloshing of water mass between two solid structures. During E1, drifter direction was predominantly upstream, dominated by tidal flood flow. E1D3 was carried out close to low tide with mean horizontal velocity less than 0.1 m/s causing deceleration of drifter clusters, hence convergence as observed with the tracks in Fig. S2. Similarly, E2D1 started at the beginning of the flood tide. However, due to the phase lag between the change in water height and change of velocity over approximately 12 min (Suara et al., 2015a), the drifters were carried downstream for about 11 min before being collected for their next deployment (Fig. 2b). During the slack water E3, resonance and reflection of flow between landmarks were likely the largest scale of fluctuation in the Eulerian flow field thus, the drifters had no prevailing drift direction.

3. Data analysis

3.1. Subsurface turbulence properties: spatial binning

Previous studies at Eprapah Creek have examined the turbulence properties at various locations near the bed using ADVs (Trevelyan et al., 2008; Chanson et al., 2012; Suara et al., 2015a). Herein, the HR drifter data are used to examine the spatial variation of turbulent properties in the subsurface layer. The LR drifter data are not included because of the large noise variance, $\sim 0.0001 \text{ m}^2/\text{s}^2$,

an order of magnitude greater than that of HR drifters, obtained from deployments made at fixed locations. The Lagrangian velocities include V_s , V_n calculated from post-processed HR drifter position time series. The dataset is converted to Eulerian measurement using a spatial binning approach, which involves a spatio-temporal averaging. The test section is divided into a number of spatial bins along the streamwise while the cross-stream data coverage (i.e. ~ 10 m from the channel centre) was not large enough to permit cross-stream binning. Therefore, the cross stream variation is ignored. For each bin, the residual velocity v_{Li} , is defined as:

$$v_i = V_i(t, s) - \langle V_i \rangle_{bin}(t, s), \quad (2)$$

where $i = s$ or n , $\langle V_i \rangle_{bin}$ is ensemble average of an instantaneous data point that falls within a bin while the corresponding eddy velocity/standard deviation of residual velocity is defined as

$$v'_i = \langle v_i^2 \rangle^{1/2} \quad (3)$$

where $\langle \rangle$ data are only considered for bins with degrees of freedom, $\text{DOF} > 4$. DOF is defined as:

$$\text{DOF}_{bin} = \frac{\sum_{j=1}^N T_j^T}{T_L} \quad (4)$$

where T^T is the total time a single drifter spends in a bin, N is the number drifters sampled within a bin and $T_L \sim 20$ s is the Lagrangian integral time scale (Suara et al., 2016b). The choice of spatial bin size, Δs , involves a compromise between resolution and statistical fidelity of velocity distribution in a bin. Herein, $\Delta s = 10$ m is obtained from sensitivity analysis such that over 95% of the data in the E1 dataset has minimum degrees of freedom, DOF of 5. Increasing Δs resulted in over-smoothing of the mean velocity while $\Delta s < 10$ m resulted in over 50% of the bin having $\text{DOF} < 5$. To reduce the bias in the statistics of the bin caused by unsteady tidal inflow, a data point can only contribute to a bin if it enters a bin within a period $\Delta T = 100$ s from time of the first data point. The mean velocity could be assumed constant for a time period equivalent to ΔT . Estimating the residual velocity with $\Delta T > 100$ s resulted in spikes in the magnitude of $\langle v'_s \rangle$, indicating the presence of large scale flow fluctuations in the v_s at some locations (e.g. 1750–1850 m streamwise — not shown) within the channel. On the other hand, $\Delta T < 100$ s resulted in a $\text{DOF} < 5$. The results were tested for stationarity and it was found that all bins were statistically stationary at a 95% confidence interval with p -values < 0.01 using Run Test (Bendat and Piersol, 2011).

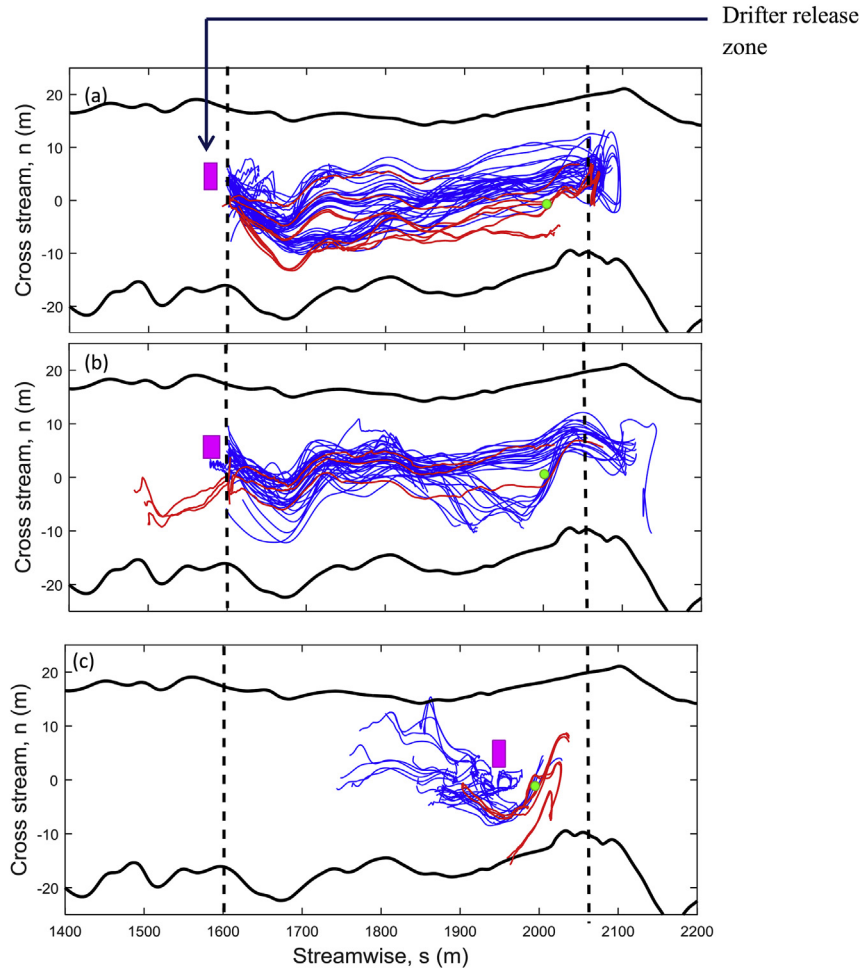


Fig. 2. Spaghetti plot of all drifter tracks for HR (red) and LR (blue) drifters and (a) E1; (b) E2; (c) E3; Purple box indicates drifter release zone; The solid black lines represent the boundary edges at typical low tide and green is the location of ADCP deployed for drifter velocity validation.

3.2. Relative dispersion analysis: pair-particle statistics

Let us consider the separation statistics of the drifters in order to establish a unique power law relationship describing dispersion with time and pair-particle diffusivity, K_p , with separation length scales. As with cluster dispersion, pair-particle dispersion is more closely tied with scalar mixing processes than single particle dispersion. A common measure to describe dispersion in this frame of reference is the mean square separation of pair particles, D_p^2 defined as:

$$D_{pi}^2(t, r_o) = \langle (r_i(t) - r_{oi})^2 \rangle - \langle (r_i(t) - r_{oi}) \rangle^2, \quad (5a)$$

$$D_p^2(t, r_o) = \frac{1}{2} [D_{ps}^2(t, r_o) + D_{pn}^2(t, r_o)] \quad (5b)$$

where i represents 's' or 'n' in the streamwise and cross stream directions, respectively, $\langle \rangle$ is ensemble average over all available pair realisations at time, t and r_o is the initial separation of a pair. D_p^2 and K_p estimates are made in bins of r_o between 0–2 m, 2–8 m, 8–16 m and >16 m. The length of deployment varies between 81 and 3961 s. In order to include the bulk of the original pairs, the analysis is considered only up to an elapsed time, $t = 1000$ s. Assuming that the flow field is stationary and that all drifters are subjected to the same motion during each experiment, the number

of realisations per cluster can be further increased by considering overlapped pair-particle segments (Brown et al., 2009). Pair particles are restarted after 50 s, i.e. more than twice the integral time scale, to allow de-correlation of particle motions (Suara et al., 2016b). For example, an original pair particle of 2000 s long would result in realisations between 0–1000 s, 50–1050 s, 100–1100 s etc., creating 20 additional realisations. This overlapping procedure reduced the variance of $D_p^2(t)$ without distorting its overall slope when compared with zero overlapping estimates. The relative (pair-particle) diffusivity, K_p in each direction is then estimated as (LaCasce, 2008; Brown et al., 2009):

$$K_{pi}(t) = \frac{1}{4} \frac{\partial D_{pi}^2}{\partial t}(t, r_o), \quad (6)$$

The scale of separation of particles, d , is defined as the geometric mean of the quantities D_{ps} and D_{pn} :

$$d(t) = \sqrt{D_{ps} \times D_{pn}}. \quad (7)$$

3.3. Relative dispersion analysis: cluster statistics

Here we estimate for each clustered drifter deployment, the apparent diffusivity (K_c), eddy diffusivities (K_{CEs} , K_{CEn}), where

applicable, and the Differential Kinematic Properties (DKP) across the clusters. This will enable a description of mixing resulting from the combination of large- and small-scale processes and identification of the dominant factors responsible transport by dispersion and mixing within the channel. Using the local s - n - u coordinate, the centroid (represented with overbar) of a cluster is defined as:

$$\bar{s}(t) = \frac{1}{N} \sum_{i=1}^N s_i(t), \quad \bar{n}(t) = \frac{1}{N} \sum_{i=1}^N n_i(t), \quad (8)$$

where i is the drifter counter and N is the total of active drifters in a cluster at time, t . The variance of an individual drifter from the centroid of the cluster is then defined as:

$$\begin{aligned} D_{cs}^2(t) &= \frac{1}{N-1} \sum_{i=1}^N [s_i(t) - \bar{s}(t)]^2, & D_{cn}^2(t) \\ &= \frac{1}{N-1} \sum_{i=1}^N [n_i(t) - \bar{n}(t)]^2. \end{aligned} \quad (9)$$

The cluster relative dispersion coefficient is calculated from the averaged variance such that:

$$K_C(t) = \frac{1}{2} \frac{\partial D_C^2(t)}{\partial t}, \quad \text{where } D_C^2(t) = \frac{1}{2} [D_{cs}^2(t) + D_{cn}^2(t)]. \quad (10)$$

The estimated diffusivity is an apparent diffusivity because it includes the effect of horizontal shear dispersion. The estimate of DKP and the separation of small-scale eddy diffusivity follows the method developed for oceanic Lagrangian data (Okubo and Ebbesmeyer, 1976). The method involves expanding the velocity components of a Taylor series about the centre of mass. The method assumes that the fluid domain is small and finite in size, velocity gradient is uniform across a cluster and cluster velocity is adequately represented in the linear term of Taylor's series (Richez, 1998). Individual drifter velocity can be described as:

$$\begin{aligned} V_s(t) &= \bar{V}_s(t) + \frac{\partial \bar{V}_s(t)}{\partial s} [s(t) - \bar{s}(t)] + \frac{\partial \bar{V}_s(t)}{\partial n} [n(t) - \bar{n}(t)] \\ &+ v_{cs}(t) \end{aligned} \quad (11a)$$

$$\begin{aligned} V_n(t) &= \bar{V}_n(t) + \frac{\partial \bar{V}_n(t)}{\partial s} [s(t) - \bar{s}(t)] + \frac{\partial \bar{V}_n(t)}{\partial n} [n(t) - \bar{n}(t)] \\ &+ v_{cn}(t) \end{aligned} \quad (11b)$$

Where \bar{V}_s and \bar{V}_n are cluster centroid velocity components obtained as time derivative of the centroid coordinates, \bar{s} and \bar{n} respectively; $\frac{\partial \bar{V}_s}{\partial s}$, $\frac{\partial \bar{V}_s}{\partial n}$, $\frac{\partial \bar{V}_n}{\partial s}$ and $\frac{\partial \bar{V}_n}{\partial n}$ are linear centroid velocity gradient terms; v_{cs} and v_{cn} are non-linear turbulence velocity terms plus measurement errors in drifter positions and velocities. These parameters are estimated using a least square approach (Okubo and Ebbesmeyer, 1976). DKPs are then described in terms of the resulting velocity gradients such that:

$$\text{Horizontal divergence } \delta(t) = \frac{\partial \bar{V}_s(t)}{\partial s} + \frac{\partial \bar{V}_n(t)}{\partial n}, \quad (12a)$$

$$\text{Vorticity } \zeta(t) = \frac{\partial \bar{V}_n(t)}{\partial s} - \frac{\partial \bar{V}_s(t)}{\partial n}, \quad (12b)$$

$$\text{Stretching deformation } a(t) = \frac{\partial \bar{V}_s(t)}{\partial s} - \frac{\partial \bar{V}_n(t)}{\partial n}, \quad (12c)$$

$$\text{Shearing deformation } b(t) = \frac{\partial \bar{V}_n(t)}{\partial s} + \frac{\partial \bar{V}_s(t)}{\partial n}. \quad (12d)$$

To identify the dominant factors responsible for the dispersion of patches and particles within the channel, a dimensionless vorticity number is employed. Truesdell's kinematic vorticity number, T_K , measures the relative importance of the vorticity field over the strain field; it is defined as:

$$T_K = \sqrt{\frac{\zeta^2}{a^2 + b^2}}. \quad (13)$$

Dispersion with $T_K > 1$ corresponds to vorticity dominance or the presence of stronger eddy-like structures whilst $T_K < 1$ corresponds to strain-field dominance or periods (regions) of convergence or divergence where dispersion is stronger (Klein and Hua, 1990; Stocker and Imberger, 2003). The minimum number of drifters required to determine the velocity gradients, centroid velocities and turbulence velocities from the least square method is four (Okubo and Ebbesmeyer, 1976).

4. Results

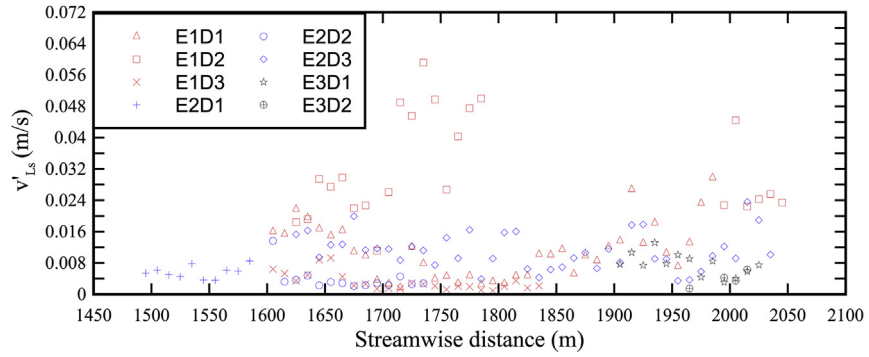
4.1. Subsurface flow turbulence properties

The surface turbulence is described in terms of the standard deviation of the residual velocity, i.e. eddy speeds ($\langle v'_s \rangle$, $\langle v'_n \rangle$), ratio of eddy speeds ($\langle v'_n \rangle / \langle v'_s \rangle$) and turbulence kinetic energy within individual bin and are presented in Fig. 3. The turbulent properties varied more strongly with tidal phase rather than the distance from the location in the streamwise direction (Fig. 3). The magnitudes of $\langle v'_s \rangle$ and $\langle v'_n \rangle$ increased with an increase tidal inflow velocity. Residual velocities observed close to at the beginning of flood tide (e.g. E2D1) were smaller than average. A discernible increase in the magnitude of $\langle v'_s \rangle$ was observed between locations AMTD, $s = 1650$ – 1800 m during flood experiment 1. This period corresponded with a phase of the tide where acceleration of flow velocity due to resonance (with period, $T \sim 3000$ s) was observed, suggesting the presence of slow fluctuation in the residual velocity. A relative increase in the magnitudes of $\langle v'_s \rangle$ and $\langle v'_n \rangle$ toward the end of the test section was likely linked with presence of secondary flow in the meander upstream. The surface flow was anisotropic with averaged eddy speed ratio per deployment varying between 0.52 and 1.1. Averaged TKE ranged between 0.41 – $12 \times 10^{-4} \text{ m}^2/\text{s}^2$. TKE increased significantly at the middle of the test section (streamwise distance, $s = 1650$ – 1800 m, E1D2), possibly linked with slow ('large-scale' eddy) fluctuations in the residual velocity and the end of the test section caused by secondary flows generated by the meander upstream.

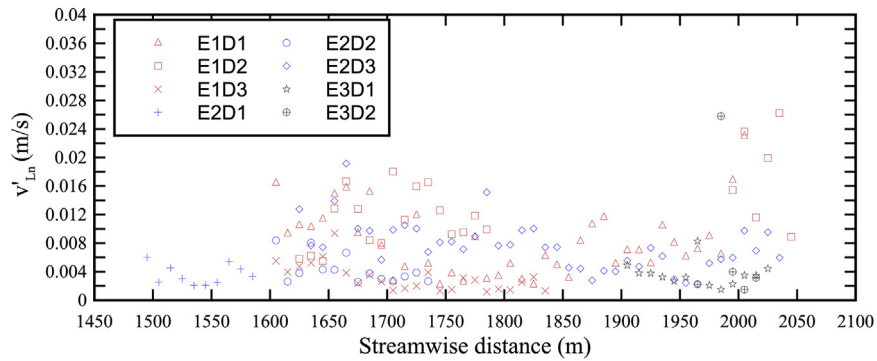
4.2. Relative dispersion

4.2.1. Relationship between cluster dispersion and pair-particle dispersion

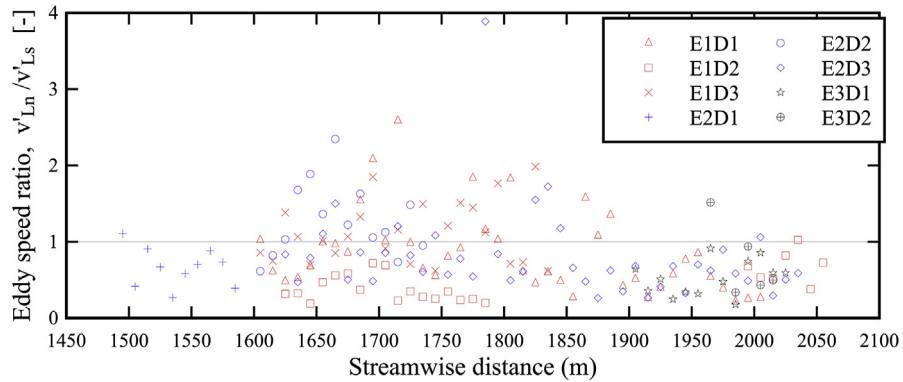
In addition to the nature of physical processes of interest and domain size, logistical and financial constraints dictate the approach by which relative dispersion and diffusivity could be estimated. Pair-particle statistics of a cluster with a fixed number of drifters results in more realisations than corresponding cluster



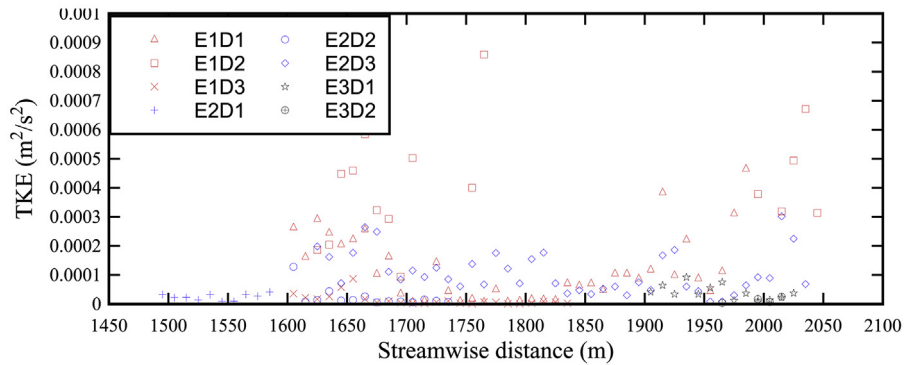
(a) Streamwise residual velocity standard deviation/‘eddy’ velocity (m/s)



(b) Cross-stream residual velocity standard deviation/‘eddy’ velocity (m/s)



(c) Eddy velocity ratios: black line indicates isotropic turbulence



(d) Turbulent kinetic energy (m^2/s^2)

Fig. 3. Subsurface flow turbulence properties as a function of location along the channel; note that the streamwise distance is positive upstream.

statistics. For example, a cluster containing five drifters would result in 10 and five realisations for D_p^2 and D_c^2 estimates, respectively. In addition, while pair-particle statistics require a number of drifters (>5), which are not necessarily deployed at the same time, cluster analysis requires a number of drifters (≥ 4) (Brown et al., 2009) concurrently deployed and active through the period of an observation (Okubo and Ebbesmeyer, 1976). Cluster statistics measure dispersion from the centroid while pair-particle statistics measure dispersion relative to each other and they are considered equivalent (LaCasce, 2008). In order to validate that the diffusivity calculated from pair-particle dispersion was equivalent that from cluster particle dispersion, a comparison was made between D_c^2 and D_p^2 calculated from Equations (5) and (9), respectively. The comparison was carried out using the HR cluster deployments during E1. Only original, non-overlapped pair particles were considered for the estimate of D_p^2 . Estimates of D_c^2 and D_p^2 were significantly correlated ($R^2 > 0.92$) at a 95% confidence interval for the three deployments (Table S1). This indicated that the pair-particle dispersion captures the behaviour within the cluster.

Due to the limited number of drifters per cluster deployed, pair-particle statistics with a larger realisation number were employed to examine the relationship describing dispersion with time and pair-particle diffusivity, K_p , with separation length scales, d , while cluster analysis was used to identify the dominant mechanism responsible for dispersion within the channel.

4.2.2. Relative (pair) particle dispersion

Fig. 4 and Fig. 5 show the relative dispersion as a function of time and relative diffusivity as a function of separation scale for different initial separation, respectively. The estimates were made from clusters (LRC1 & LRC2) for deployments in E1 (i.e. E1D1, E1D2 and E1D3). Note that d reflects the spatio-temporal growth of a patch because the original separation, r_o , is removed from D_p so that the scale dependence of diffusivity is similar to those in literature, where $K_p \sim l^l$ (where, $l = d^2 + r_o$) (Richardson, 1926; Brown et al., 2009). In general, the particles travelled along similar streamlines subject to some underlying small-scale turbulence. At large separations, the particles experienced dispersion induced by shear and larger-scale fluctuations. For all initial separation, streamwise dispersion grew with a power between 1.5 and 2. The side

boundary suppressed the spreading in the cross stream, reducing the growth of dispersion close to power of 1, within an elapsed time of 30 s. The result of diffusivity shows that, with the exception of the large initial separation ($r_o > 16$ m), the K_p values showed no discernible dependence on the initial separation, r_o . K_p values were noisy but exhibited dependence on a separation scale not significantly deviated from Richardson's 4/3 power law.

Mean square pair-particle separation, D_p^2 , and diffusivity, K_p , were obtained separately for each cluster and deployment using all initial separation, r_o , of original and overlapped realisations. The average diffusivity for all deployments flood tide E1, K_{ps} ranged from 0.001 to 2 m^2/s and K_{pn} ranged between 0.0002 and 0.004 m^2/s in the streamwise and cross-stream directions, respectively. A similar range of values was observed during flood tide E2 while K_p varied between 0.02–0.28 m^2/s and 0.002–0.006 m^2/s for the streamwise and cross-stream directions, respectively, during the slack tide E3. The large diffusivity range (~ 3 orders of magnitude) reflects the broad range of scales (large and small scales) responsible for dispersion during a typical flood tide.

Fig. 6 shows the dispersion for the different experiments (E1, E2 and E3). For comparison with Richardson's power law relationship, $D_p^2 \sim t^\alpha$, the dispersions are plotted alongside dashed-lines in the form $D_p^2 \sim t^\alpha$ for $\alpha = 1, 2$ and 3. For each experiment, clusters with the similar drifter designs (length and diameter) and deployments were combined. However, there was no discernible difference between the dispersion among the clusters. This could be linked with the fact that the water columns were reasonable well-mixed during the drifter experiments as observed with similar magnitudes of conductivity measured both next to the bed and the free surface (Fig. S1). Dispersion was weakest during the slack water. In general, dispersion in the streamwise direction was consistently greater than that in the cross-stream direction indicating anisotropic dispersion due to the limited channel width and dominant streamwise flow direction. The LR clusters formed a circular patch (i.e. $D_{ps} = D_{pn}$) at elapsed time $t < 100$ s during the slack water, suggesting that a reduced stretching effect on the streamwise dispersion compared to the flood experiments. The cross-stream dispersion reduced toward an asymptote after an elapsed time, $t > 300$ s, due to suppression from channel banks. Visual inspection of the power fits indicated that the dispersion in the streamwise

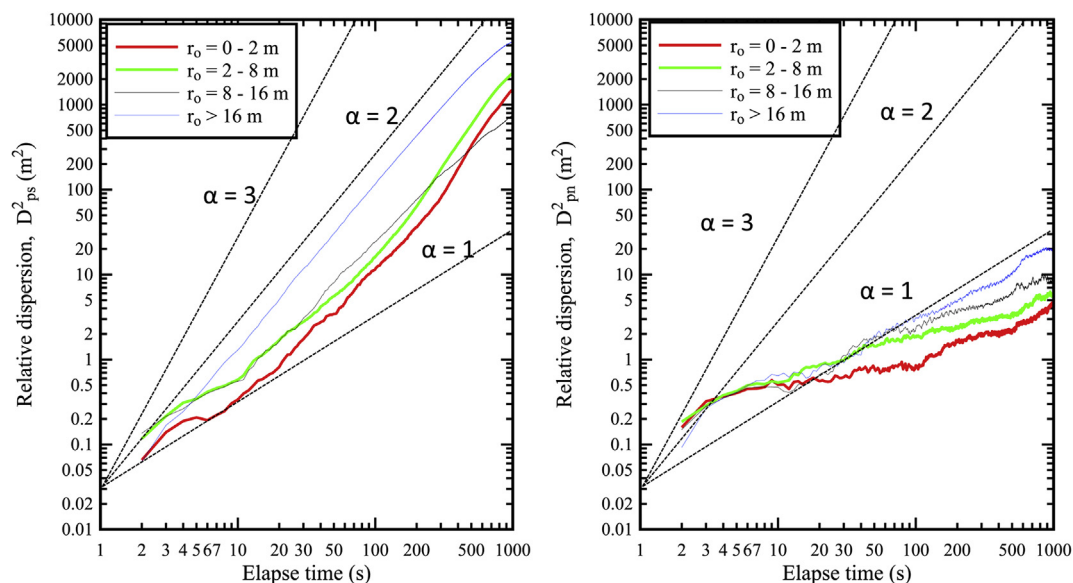


Fig. 4. Dispersion as a function of elapsed time, t for non-overlapped estimates from LR clusters 1 and 2 during E1D1, E1D2, E1D3; (a) Streamwise (b) Cross-stream directions; Black slant-dashed lines correspond to power law relationship in the form $D_p^2 \sim t^\alpha$ with $\alpha = 1, 2$ and 3.

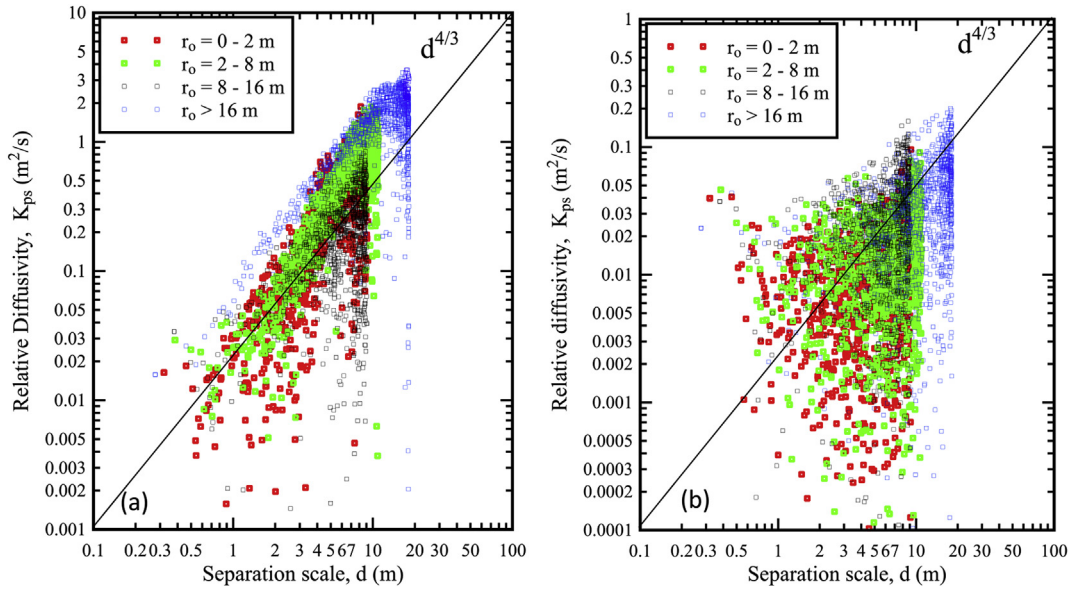


Fig. 5. Relative diffusivities as a function of separation length scale, d for non-overlapped estimates from clusters (LRC1 & LRC2) during E1D1, E1D2, E1D3; (a) Streamwise (b) Cross-stream directions; Black slant lines correspond to Richardson's $4/3$ power law scale; Note the difference in scale on the vertical axes.

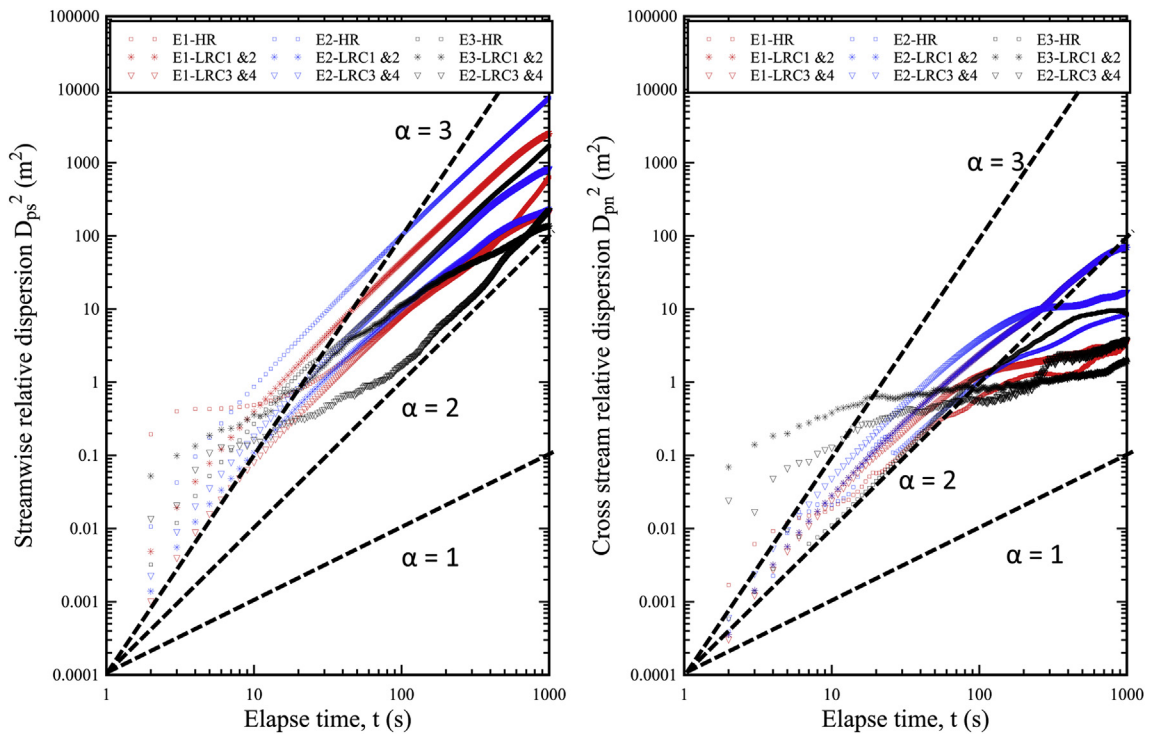


Fig. 6. Pair-particle dispersion against time for the three different experiments for different clusters (i.e (1) HR (2) LR C1 & C2; (3) LR C3 & C4); E1 in red; E2 in blue; and E3 in black; Black slant-dashed lines correspond to power law relationship in the form $D_p^2 \sim t^\alpha$ with $\alpha = 1, 2$ and 3 .

directions grew with time, with power ranging from 1.5 to 2. Dispersion in the cross-stream direction was more suppressed and varied with time to the power closer to 1. Fig. 7 shows the relative diffusivity for different experiments. The diffusivity dataset from the LR drifters at slack water experiment E3 were noisy at small scale due to relatively large position accuracy of the instrument compared with the displacement during E3 experiment and are not shown in Fig. 7. The relative diffusivity plots for all experiments are presented in the Supplementary Fig. S3. At the small-length scales

($d < 0.5$ m), the diffusivity follows Richardson's $4/3$ power law closely. The diffusivity grew weaker as the separation scale increased with scaling power, $\gamma \sim 0.8-1$ (Fig. 7). Diffusivity decorelated with length scale at large separation ($d > 2$ m) scales and became noisy, likely because of the random effect of smaller-scale processes on the large separation. The relative diffusivities in the streamwise direction were an order of magnitude larger than in the cross-stream direction.

A power law relationship in the form $D_p^2 \sim t^\alpha$ was sought to

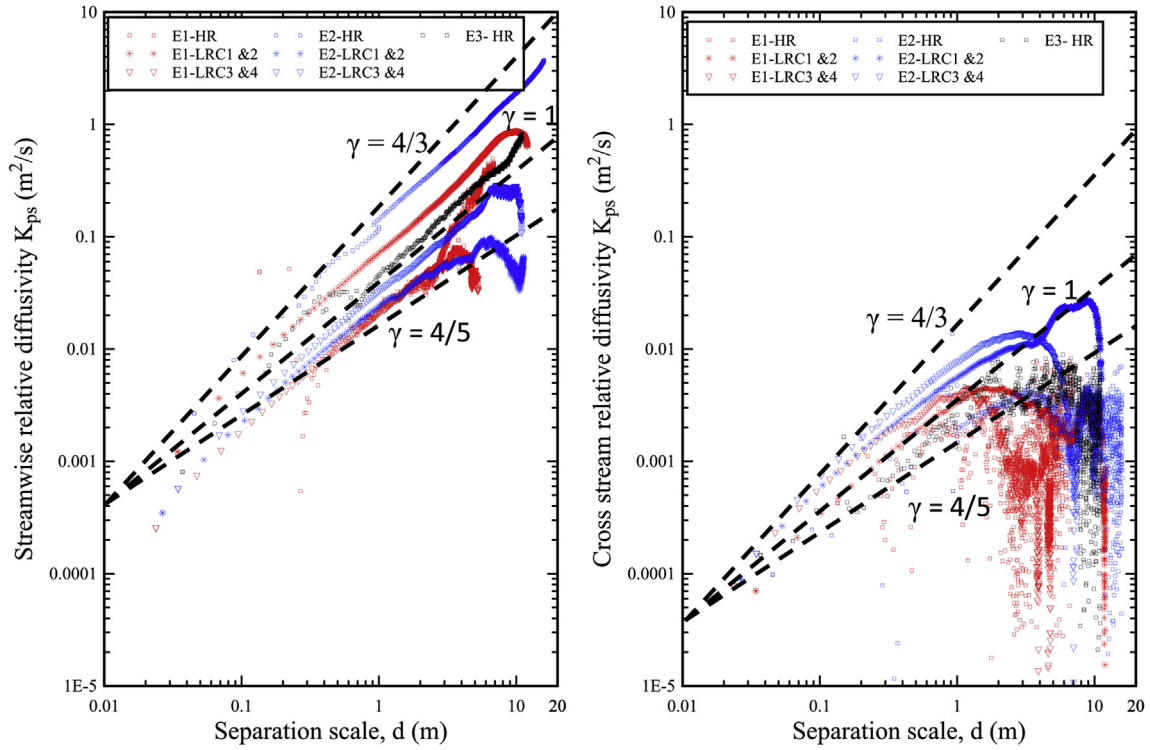


Fig. 7. Relative diffusivities as a function of separation length scale, d , for the three different experiments for different clusters; (i.e. (1) HR (2) LR C1 & C2; (3) LR C3 & C4); E1 in red; E2 in blue; and E3 in black; Black slant-dashed lines correspond to power law relationship in the form $K_p \sim d^\gamma$ with $\gamma = 4/3, 1$ and $4/5$.

describe the dispersion within the channel. For each experiment, all initial pair particles and realisations from cluster from physically similar drifters were employed. The initial dispersion regime was similarly described by estimating the powers (α_s, α_n) of the least square fitting using elapsed times, $t = 0-20$ s, i.e. order of one integral time scale. These results are tabulated (Table 2). For the flood tide experiments, α was initially larger with $\alpha_s = 1.2-2.1$ and $\alpha_n = 1.3-2.1$ (Table 2, Column 4 and 6, respectively), compared with their corresponding overall dispersion rate (Table, Columns 5 and 7, respectively). At slack tide, the power law relationship reflected a reduction in spreading rate with $\alpha_s = 0.9-1.7$ and $\alpha_n = 0.7-2.2$ at the initial stage while spreading in the later stage was enhanced in the streamwise direction. Spreading in the cross-stream direction was suppressed in the later stage by the banks while proximity to solid boundaries and reflection from internal resonances were the likely cause for the suppression along the streamlines. For all experiments, the average pair-particle separation can be described as

a power law relationship with $\alpha_s \sim 1.83$ and $\alpha_n \sim 0.8$. The dispersion in the streamwise direction reflected a ballistic behaviours indicating that the particle-pairs behaved as independent particles. The dispersion in the cross stream direction was weaker and showed behaviour close to a diffusive dispersion regime at time longer than the integral time scale, $T_L \sim 20$ s.

Similarly, a power relationship in the form of $K_p \sim d^\gamma$ was investigated to describe the relative diffusivity. As shown in Fig. 5, the K_p values were noisy at large separation scale, d , due to de-correlation of length scale and diffusivity. Therefore the power law fit was only determined within the small scale ($t < 100$ s). Note that power law fits resulting in a R^2 -values < 0.9 are not included in the result summarised in Table 2. For all of the experiments, the diffusivity may be described as $K_p \sim d^\gamma$ with $\gamma_s \sim 1.01$ and $\gamma_n \sim 0.85$ in the streamwise and cross-stream directions, respectively for separation scale ranging from 0.1 to 10 m. The relationship reflected a slightly weaker diffusivity within the channel compared with

Table 2
Summary results of pair dispersion analysis for different experiments and clusters; Power law fits are made for initial dispersion case (i.e. $t \leq 20$ s) and all ($t \leq 1000$ s) through least square estimate^a; V_c is the mean cluster horizontal velocity magnitude.

Exp #	Cluster	N_R	α_s		α_n		K_{ps} (m^2/s)	K_{pn} (m^2/s)	V_c (m/s)	γ_s	γ_n
			$t = 20$ s	all	$t = 20$ s	all					
E1	HR	504	1.19	2.53	1.79	0.77	0.40 ± 0.3	0.004 ± 0.004	0.19	1.06	0.92
	CL1 & 2	1388	2.14	1.55	2.06	0.84	0.63 ± 0.2	0.002 ± 0.001	0.17	1.1	0.81
	CL3 & 4	666	2.12	1.18	2.07	0.42	0.05 ± 0.02	0.001 ± 0.001	0.17	1.0	0.75
E2	HR	294	2.06	1.83	1.28	0.83	1.93 ± 1.0	0.002 ± 0.001	0.13	1.11	–
	CL1 & 2	1320	2.12	1.05	2.12	1.3	0.06 ± 0.02	0.02 ± 0.02	0.13	0.86	0.88
	CL3 & 4	680	2.14	1.37	2.11	0.53	0.21 ± 0.07	0.004 ± 0.004	0.16	0.97	0.88
E3	HR	96	1.65	1.82	2.15	0.66	0.1–0.28	0.002–0.003	0.06	1.0	–
	CL1 & 2	1028	1.03	1.01	0.79	0.40	0.04 ± 0.02	0.02 ± 0.01	0.03	–	–
	CL3 & 4	920	0.91	2.30	0.71	0.64	0.06 ± 0.05	0.004 ± 0.003	0.05	–	–

^a Values reported here have squared correlation coefficient, $R^2 > 0.90$. N_R is the number of pair-particle realisations.

Richardson's scale, with $\gamma = 1.33$. The results indicated that although the diffusivity at small scale ($d < 0.5$ m) follows Richardson's law, diffusivity at larger scales was weaker.

4.2.3. Relative (cluster) dispersion

While the relationships established through pair-particle analysis have practical application in particle transport modelling and parametrising the sub-grid diffusivity as a function of length scale in numerical models, there is a need to identify the dominant mechanism governing the transport of particles. Herein, the behaviour of drifter clusters is discussed in relation to possible underlying physical factors. Fig. 8 shows the patch formed by different clusters deployed within 10 min of each other during E1D1. The patch location and size are represented by an ellipse with axes D_{cs} and D_{cn} in the streamwise and cross-stream directions. The results highlighted strong variation within the different clusters. Their initial deployment memory was quickly lost after which the cluster behaviours were likely influenced by their sizes, local flow variation and proximity to boundaries. After approximately 100 s, clusters were stretched along the streamwise direction and contracted along the cross stream, suggesting an influence from banks. Clusters converged in the cross-stream direction on approaching the banks.

A single deployment resulted in a range of cluster diffusivities, K_c , values and the data varied with the instantaneous effective cluster size, D_c . Because of the limited number of drifters in each individual cluster, K_c values obtained from Equation (4) were noisy. Therefore, only the mean values over cluster deployments are reported in Table 3. The definition of cluster allows negative values of diffusivity, which indicate cluster contraction, i.e. clustering rather than spreading. Diffusivities resulting from spreading and contraction are separately averaged for individual cluster and are determined by taking the mean of a deployment duration.

The cluster diffusivity estimates, K_c are presented in Table 3, Columns 6 and 7 for spreading and contraction cases, respectively. For E1, the spreading K_c ranged between 0.05 and 3.01 m^2/s while that of contraction ranged between -0.06 and -4.2 m^2/s . In flood E2, K_c ranged between 0.01–0.66 m^2/s for spreading and -0.02 – -0.79 m^2/s for contraction. Conversely, slack water E3 experienced a smaller magnitude of K_c with values ranging between 0.05–0.25 m^2/s and -0.05 – -0.28 m^2/s for spreading and contraction respectively. The cluster diffusivity increased with streamwise velocity during the flood and had low values similar to those at slack water for deployments made during low flows (e.g. E1D3 and E2D1 Table 3). Note that the clusters were taken ebbward during E2D1. This observation is similar to the previous study on the effect of tide on diffusivity, in which eddy diffusivity was observed to increase with the tidal velocity (Suara et al., 2016b). The large values of diffusivity are typical of large

streamwise separation, possibly caused by some drifters in a cluster being stretched out near the bank or secondary flow in the meander next to the end of the test section.

Negative diffusivity values indicating contraction of cluster were observed at different locations during the field experiments. During the flood experiment E1, contraction of drifters occurred predominantly between locations AMTD, $s = 2000$ – 2100 m, i.e., the end of the test section. This was likely influenced by the transverse velocity shear resulting from the presence of meander immediately upstream the test section (locations AMTD, $s = 2200$ m). During the flood experiment E2, contraction of drifters occurred predominantly between locations AMTD, $s = 1750$ – 1900 m during deployments E2D2 and E2D3. This may be associated with the proximity of the centroid of related drifters to the channel banks among other factors.

4.2.3.1. Differential kinematic properties and small-scale diffusivity.

The objective here is to examine the dominant mechanism responsible for particle transport within the channel at time scales less than that of a tide. This is done using two separate approaches. First, the relative significance of vorticity through Truesdell's kinematic vorticity number, T_K , is examined (Truesdell, 1954). Mean DKP values were in the order of 10^{-3} s^{-1} . The standard deviation of DKP was, on average, an order on magnitude greater than the mean, indicating large variability and a limited number of particles in the clusters. For all of the clusters and deployments, the time variation of T_K was predominantly less than 1, suggesting that dispersion of the clusters was dominated by strain fields rather than eddy-like structures. However, $T_K > 1$ were observed at the meanders towards the end of the test section. The dominance of the strain field within the channel implies that water parcels and scalar are stretched and sheared horizontally streamwise. This was likely associated with horizontal velocity shears resulting from the interactions of the tide with topographical structures within and outside the channel.

Another method of quantifying the dominant processes within the channel is to measure the relative contributions of large- and small-scale processes through the ratio of apparent and eddy diffusivities. The eddy diffusivities (K_{CEs} , K_{CEn}) for each cluster are estimated by the analogy of the mixing length theory and turbulence theory as (Obukhov, 1941; Okubo and Ebbesmeyer, 1976):

$$K_{CEs}(t) = c \sigma_{vs}(t) D_{cs}(t), \quad K_{CEn}(t) = c \sigma_{vn}(t) D_{cn}(t), \quad (14)$$

$$\sigma_{cs}^2(t) = \left[\frac{1}{N-1} \sum_{i=1}^N v_{csi}^2(t) \right], \quad \sigma_{cn}^2(t) = \left[\frac{1}{N-1} \sum_{i=1}^N v_{cni}^2(t) \right] \quad (15)$$

where c is the constant of proportionality in the order of 0.1 (Okubo and Ebbesmeyer, 1976; Manning and Churchill, 2006), σ_{cs} & σ_{cn} the standard deviations of turbulence velocities, and D_{cs} & D_{cn} the standard deviations of the drifter displacement from the centroid (i.e. patch length scale). For the estimate to be reliable, it is necessary that the standard deviation of turbulence velocities is significantly greater than the inherent noise. For all deployments and clusters, σ_{cs} & σ_{cn} were in the order of 0.01 m/s. The standard deviation of inherent velocity error estimated from post-processed drifter datasets obtained from fixed positions was an order of magnitude lower than σ_{cs} & σ_{cn} obtained from the field (moving) deployments for the HR drifters. However, the magnitude of the inherent velocity error was not significantly different to σ_{cs} & σ_{cn} obtained from the field (moving) deployments for the LR drifters. Therefore the LR drifters employed in this study were considered unsuitable for estimates of small-scale processes within the

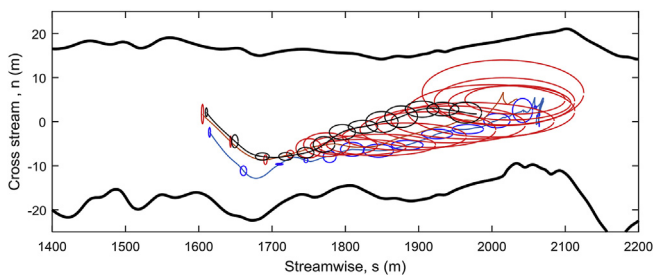


Fig. 8. Representative tracks formed by instantaneous centroid locations of clusters, HR (blue); C1 (red) and; C3 (black) for E1D1; Overlaid are cluster size formed by corresponding ellipse (see text) at 120 s time steps; The solid black lines represent the boundary edges at typical low tide.

channel and the results are not presented.

The eddy diffusivity from the HR drifter clusters for E1D1 and E1D2 $\sim 0.02 \text{ m}^2/\text{s}$ and $\sim 0.001 \text{ m}^2/\text{s}$ in the streamwise and cross-stream directions, respectively. These values are consistent with eddy diffusivity range of 0.001 and $0.02 \text{ m}^2/\text{s}$ estimated from single dispersion analysis during a flood tide experiment at Eprapah Creek (Suara et al., 2016b) and larger than Eulerian vertical eddy viscosities, ν_T within $10^{-5} < \nu_T < 10^{-3} \text{ m}^2/\text{s}$ reported in Treveltham (2008). For the two flood deployments, the effective cluster diffusivities, K_c , resulting from combinations of large- and small-scale processes, are one to two orders of magnitude greater than the average eddy diffusivities related to small-scale processes. This further indicates that large-scale processes (e.g. horizontal shear) are the dominant mode of dispersion within the channel at time scales less than a tidal period.

5. Discussion

Eprapah Creek is a coastal type tide-dominated estuary which discharges into Moreton Bay, a semi-protected bay that isolates the estuary from the rest of the coast. Moreton Bay is characterised with the presence of topographical structures such as islands (e.g. Sand Island and Peel Island) which impose additional spatio-temporal variability on the tidal velocity. In addition, the estuary is funnel-shaped with meanders, bends and rough bathymetry. These features create large scale horizontal shear velocity in addition to the bed generated turbulence. The existence and the interaction between these scales of motion were suggested to significantly increase the magnitudes of horizontal dispersion coefficient in tide-dominated estuary (Zimmerman, 1986; Tseng, 2002; Treveltham, 2008). Quantifying and understanding the behaviour of clustered particles is important for accurate modelling and prediction of particle transport such as larvae transport and pollutant tracking in similar water bodies. Lagrangian drifters were deployed in Eprapah Creek to examine the dynamics of the surface flow and dispersive behaviour of these scales of fluctuation in the Eulerian flow field.

5.1. Turbulence characteristics of the surface flow

Turbulence properties are required for accurate parameterising turbulence effect in numerical models. To examine the surface turbulent properties, the Lagrangian velocities were transformed into Eulerian velocity using spatial binning. The results show that surface turbulence characteristics exhibited spatio-temporal variation. The eddy velocities suggested the surface turbulence were more dependent on the phase of the tide than the distance from the mouth. The eddy velocities increased with increase in the horizontal mean velocity. However, some large values of eddy velocities were observed at the end of the test section, close to the meander. This was likely linked with the secondary flow developed next to the meander. The eddy velocity ratio (i.e. anisotropy) $\langle v'_n \rangle / \langle v'_s \rangle$ varied between 0.52 and 1.1. This was similar to the values observed next to the bed where $\langle v'_n \rangle / \langle v'_s \rangle \sim 0.5\text{--}0.96$ was observed (Treveltham et al., 2008; Suara et al., 2015a) and in a straight prismatic rectangular channel in the laboratory where $\langle v'_n \rangle / \langle v'_s \rangle \sim 0.5\text{--}0.7$ (Nezu and Nakagawa, 1993). The averaged TKE ranged between $0.41\text{--}12 \times 10^{-4} \text{ m}^2/\text{s}^2$ and have similar average values as those obtained from the ADV next to the bed.

The eddy velocities and kinetic energy increased with the increase in the tidal inflow velocities. Some instances of rapid increase in turbulence kinetic energy likely caused by slow ('large scale' vortices) fluctuations were observed. Secondary flow caused by meander also increased the turbulence energy at locations close to the end of the test section. Consistent with previous Eulerian

observations near the bed, the surface flow was anisotropic with averaged eddy velocity ratio per deployment varying between 0.52 and 1.1.

5.2. Dispersion and diffusivity with scales

The dispersion and diffusivity are examined using the pair-particle separation and cluster statistics which were found correlated. The relative diffusivity estimated from pair-particle separation showed that the flood tides contained broader range of scales, thus higher diffusivity than the slack. Similarly, the mean effective cluster diffusivity for the spreading clusters varied with the tidal inflow velocity. This observation was consistent with the linear relationship obtained between eddy diffusivity and tidal inflow from single dispersion analysis of drifter within Eprapah (Suara et al., 2016b). Cluster diffusivity ranged between $0.01\text{--}3.01 \text{ m}^2/\text{s}$ for spreading clusters and $-0.06\text{--}4.2 \text{ m}^2/\text{s}$ for contracting clusters. The average diffusivity for the two flood tides, $K_c = 0.51 \text{ m}^2/\text{s}$ is similar to $K_c = 0.5 \text{ m}^2/\text{s}$, obtained in a similar independent drifter experiment at a tidal inlet (Spydell et al., 2015). The estimates were consistent with the value of dispersion coefficient of $0.57 \text{ m}^2/\text{s}$ obtained from absolute dispersion of during a peak flow under a neap tidal condition in Eprapah Creek (Suara et al., 2016b).

The lower values of the cluster diffusivities observed in this study were within the minimum lateral diffusivity, $K_{nn} = 0.003\text{--}0.42 \text{ m}^2/\text{s}$ obtained from dye tracer studies, particularly in similar shallow rivers and estuaries (depth $< 5 \text{ m}$) such as Cardiff Bay, Loch Ryan, Forth Estuary, Humber Estuary in the United Kingdom and Saone in France (Riddle and Lewis, 2000; Suara et al., 2016b). The upper values of the cluster diffusivities were similar to $K_{ss} = 6.5\text{--}9.9 \text{ m}^2/\text{s}$ observed from dye tracer studies in natural rivers (depth = $0.58\text{--}1.56 \text{ m}$; width = $20\text{--}40 \text{ m}$) such as Green-Dumanish River, Powell River (Table 5.3; Fischer et al. (1979)). A wider comparison of drifter diffusivity observed in Eprapah Creek and dye tracer estimates in similar water bodies is presented elsewhere (Suara et al., 2015b, 2016b).

Clustering (i.e. contraction of cluster) of buoyant particles as against spreading has been observed in environmental flows such as estuarine embayment and nearshores (Manning and Churchill, 2006; Stevens, 2010). This phenomenon is usually related to combination of physical processes governing the Eulerian flow field and dynamics of the particles in a turbulent flow influenced by their inertia and drag (Pinton and Sawford, 2012). Convergence of drifter clusters have been reported to be caused by proximity to tidal fronts (Manning and Churchill, 2006). Internal waves and oscillatory residual velocities have also been shown to correlate with periods of convergence of drifter clusters (Stocker and Imberger, 2003; Suara et al., 2016a). Convergence resulting from clusters entering deeper water and stratification (List et al., 1990; Stevens, 2010) are not clearly evident in the present study because the channel did not exhibit a significant depth difference within the section studied (Fig. 1) while the water column was fairly well mixed during the experiments (Fig. S2). Contraction of 2D surface velocity observations resulting from underlying 3D effect can inherently lead to convergence of surface drifter clusters (Kalda et al., 2014). In natural channels, secondary flow cells characterised with strong transverse velocity shears greatly influence clustering of floating particles at meanders (Hey and Thorne, 1975). Observations from ADV at the meander upstream the experimental domain have shown evidence of strong secondary flows at high, ebb and flood tides within Eprapah Creek (Chanson et al., 2012).

In the present study, clustering was observed close to meanders and banks which is consistent with the dominance of strain field (combination of shear and strain deformations) observed with the cluster dynamics. This was likely further enhanced by the

Table 3
Cluster relative diffusivity and turbulent eddy diffusivities.

Experiment number	Deployment number	Cluster ID	Number drifters	Duration (s)	Effective K_c Spreading (m^2/s)	Effective K_c Contracting (m^2/s)	Eddy K_{CES} (m^2/s)	Eddy K_{CEn} (m^2/s)	Divergence δ (s^{-1}) $\times 10^{-3}$	Vorticity ζ (s^{-1}) $\times 10^{-3}$	Shearing, b (s^{-1}) $\times 10^{-3}$	Stretching, a (s^{-1}) $\times 10^{-3}$	Truesdell's number T_k
E1	D1	HR	4	1799	0.81	-0.11	0.0213	0.0016	3.38	-5.23	3.62	-1.53	0.75 \pm 0.54
		LRC1	5	1801	0.34	-0.32	—	—	1.14	4.01	-3.95	1.74	0.96 \pm 0.92
		LRC2	4	1591	0.16	-0.15	—	—	3.72	6.27	-3.32	-1.05	1.03 \pm 0.81
		LRC3	5	1436	0.49	-0.59	—	—	0.33	-1.50	2.86	1.85	0.83 \pm 0.36
	D2	LRC4	4	1311	0.16	-0.16	—	—	0.59	1.50	-0.58	1.54	0.61 \pm 0.89
		HR	4	1801	0.15	-0.18	0.0148	0.0008	-0.78	-12.59	11.95	2.44	0.77 \pm 0.52
		LRC1	5	2101	3.09	-4.20	—	—	2.98	-3.83	2.45	0.79	0.79 \pm 0.35
		LRC2	4	2101	1.57	-2.22	—	—	2.79	-11.36	15.80	2.80	0.95 \pm 0.86
	D3	LRC3	5	1501	0.63	-0.57	—	—	2.40	-2.64	1.82	-0.31	0.78 \pm 0.36
		LRC4	4	1381	0.37	-0.43	—	—	3.11	-12.27	13.86	2.93	0.78 \pm 0.36
		HR	3	3961	—	—	—	—	—	—	—	—	—
		LRC1	5	2821	0.05	-0.06	—	—	1.42	-2.26	1.94	1.07	0.82 \pm 0.32
		LRC2	4	2221	0.15	-0.11	—	—	3.12	7.02	-6.64	4.13	0.74 \pm 0.57
		LRC3	5	1921	0.07	-0.10	—	—	1.66	-5.23	3.99	0.07	0.83 \pm 0.57
		LRC4	4	1621	0.05	-0.10	—	—	1.52	-3.05	2.86	0.56	0.89 \pm 0.49
		E2	D1	HR	3	—	—	—	—	—	—	—	—
LRC1	5			1441	0.01	-0.02	—	—	-0.35	-1.40	1.03	2.68	0.84 \pm 0.49
LRC2	4			421	—	—	—	—	-4.08	2.12	-2.78	2.78	0.60 \pm 0.24
LRC3	5			81	—	—	—	—	-1.30	-0.44	-0.65	-2.04	0.29 \pm 0.15
D2	LRC4		4	81	—	—	—	—	1.00	0.12	-0.64	0.61	0.63 \pm 0.55
	HR		3	—	—	—	—	—	—	—	—	—	—
	LRC1		5	2549	0.53	-0.63	—	—	4.16	-0.48	0.43	3.50	0.49 \pm 0.50
	LRC2		4	2256	0.46	-0.63	—	—	4.57	0.73	1.28	1.25	0.72 \pm 0.58
D3	LRC3		5	2871	0.56	-0.73	—	—	5.60	7.96	-8.06	5.57	0.76 \pm 0.72
	LRC4		4	1911	0.66	-0.79	—	—	7.94	3.86	-4.79	6.11	0.89 \pm 0.96
	HR		3	—	—	—	—	—	—	—	—	—	—
	LRC1		5	2761	0.23	-0.24	—	—	1.40	0.81	-0.44	1.16	0.79 \pm 1.90
	LRC2		4	2701	0.30	-0.24	—	—	1.36	-1.61	3.53	0.88	0.93 \pm 0.91
	LRC3		5	2281	0.79	-1.10	—	—	2.18	-13.02	12.17	2.77	0.95 \pm 0.15
	LRC4		4	2281	0.18	-0.10	—	—	-0.53	-2.84	1.92	1.43	0.67 \pm 0.90
	E3		D1	HR	3	—	—	—	—	—	—	—	—
LRC1		5		1981	0.25	-0.28	—	—	-9.62	-27.93	26.64	-9.35	0.90 \pm 0.26
LRC2		4		1801	0.05	-0.06	—	—	9.52	97.09	-66.83	72.53	0.87 \pm 0.61
LRC3		5		2281	0.21	-0.05	—	—	1.39	0.36	-2.19	0.44	0.84 \pm 0.85
LRC4		4		2101	0.18	-0.18	—	—	0.59	-12.49	13.66	0.51	1.79 \pm 0.53

horizontal velocity shear cells manifested as slow fluctuations in the velocity field, and finite size of the drifters. Separation of these effects to examine the main mechanism would however require further investigation.

The pair-particle statistics, D_p and K_p relative to d and t were calculated for different tidal conditions. The dispersion within the channel was similar for the two flood tides while dispersion during the slack water was weaker. The pair-particle dispersion, D_p^2 , scales as $D_p^2 \sim t^{1.83}$ and $D_p^2 \sim t^{0.8}$ in the streamwise and cross stream directions respectively for all the experiments. The observed relations indicate that the dispersion within the channel was weaker than Richardson's dispersion with $\alpha = 3$, while the streamwise dispersion was stronger than those observed in rip beaches where $\alpha \sim 1.33$ – 1.5 were observed (Brown et al., 2009). For all of the experiments, diffusivity can be described as $K_p \sim d^\gamma$ with $\gamma_s \sim 1.01$ and $\gamma_n \sim 0.85$ in the streamwise and cross-stream directions, respectively for separation scale ranging from 0.1 to 10 m. The relationship reflected a weaker diffusivity within the channel compared with Richardson's scale, with $\gamma = 1.33$. The diffusivity relationships here are similar with those observed in small- to medium-sized lakes with $\gamma \sim 1.1$ for length scale ranging from 10 – 10^5 m and stronger than those $\gamma \sim 0.1$ – 0.2 with length scale ranging from 1 to 10 m in rip current beaches (Brown et al., 2009).

Mean DKP values were in the order of $10^{-3} s^{-1}$. Observed mean values were an order of magnitude larger than those observed in a tidal embayment (Stevens, 2010) and two orders of magnitude larger than observed in a non-tidal lake (Stocker and Imberger, 2003). The large mean estimates likely reflected the faster

circulation in Erapah Creek with mean speed up to 0.4 m/s (Fig. S2) when compared with those obtained in the tidal embayment where the mean velocity magnitude was limited to 0.05 m/s and the non-tidal lake which was wind-driven (Stocker and Imberger, 2003; Stevens, 2010).

5.3. Dominant mechanism governing dispersion in the channel

The diffusivity reported herein are orders of magnitude larger than the horizontal eddy diffusivity obtained with high resolution drifters and the vertical diffusivity scale estimates using high frequency sampled acoustic Doppler velocimeter in Erapah Creek (Trevethan and Chanson, 2009; Suara et al., 2015b). The presence of large scale fluctuations in Eulerian velocity field could result into horizontal shear current. This might interact with the bed generated turbulence to result into a typical large horizontal diffusivity in a tidal system. Two independent methods were used to investigate the relative contributions of turbulence and the strain fields (i.e. shearing and stretching) in the observed diffusivity. The eddy diffusivity estimates of 0.02 and 0.001 m^2/s in the streamwise and cross stream directions respectively, were obtained from the high resolution drifter clusters using Okubo's method. These values were two orders of magnitude smaller than the average cluster apparent diffusivities. In addition, dimensionless vorticity indicated mean values $T_k > 1$ for all drifter deployments. This indicated the dominance of strain fields, i.e. large scale processes such as horizontal shear in the cluster dynamics under the period and study conditions.

6. Conclusions

The presence and interaction of large scale velocity shear with the turbulence in tidal estuaries are often the cause of large horizontal diffusivity. The interactions of tides with the internal structures of the estuarine channel and in the adjacent bays usually induce horizontal velocity shear in the Eulerian flow field. To investigate the dynamics of surface flow in a relatively small shallow tidal estuary at time scales less than a tidal period, GPS-tracked drifters were deployed in clusters of four and five, over three field experiments comprising of two flood and one slack tides. The results show that surface turbulence characteristics exhibited spatio-temporal variation similar to the characteristic of the bed generated turbulence. The eddy velocities and kinetic energy increased with the increase in the tidal inflow velocities. Secondary flow caused by meander increased the turbulent kinetic energy within the channel. The surface flow was anisotropic with averaged eddy velocity ratio per deployment varying between 0.52 and 1.1.

Key results of the investigation are the presence of broad range of dispersion scale within a short time period, less than a tidal cycle and the observation of anomalous sub-diffusive behaviour within the micro-tidal estuary. The large diffusivity range (over 3 orders of magnitude) reflects the broad range of scales (large and small scales) responsible for dispersion during a typical flood tide. In addition, the study indicated dispersion were weaker than Richardson's scale as pair-particle dispersion, D_p^2 scales as $D_p^2 \sim t^{1.83}$ and $D_p^2 \sim t^{0.8}$ in the streamwise and cross stream, directions respectively. At small separation scale, pair-particle ($d < 0.5$ m) diffusivity follows Richardson's 4/3 power law and grew weaker with increase in separation scale. The overall diffusivity scaled as $K_p \sim d^\gamma$ with $\gamma_s \sim 1.01$ and $\gamma_n \sim 0.85$ in the streamwise and cross-stream directions, respectively for separation scale ranging from 0.1 to 10. Two independent methods were used to investigate the relative contributions of turbulence and the strain fields (i.e. shearing and stretching) in the observed diffusivity. The cluster and turbulent eddy diffusivities determined from the Okubo and Ebbesmeyer methods alongside Truesdell's kinematic vorticity number clearly revealed the dominance and importance of horizontal strain fields (shearing and stretching) in the spreading of particles with the channel.

Acknowledgments

The authors acknowledge the contributions of a volunteer group of second-year students from the University of Queensland and volunteer undergrads from Queensland University of Technology — Madeline Brown, Daniel Maris and Tim Ketterer — in the field data collection. They also acknowledge the support received from Dr Badin Gibbes, Dr Helen Fairweather, Dr Charles Wang, Dave McIntosh and Dr Hang Wang in planning, implementing the field study and data analysis. The authors thank the Queensland Department of Natural Resources and Mines, Australia, for providing access to the SunPOZ network for reference station data used for RTK post processing of the HR GPS-tracked drifter. The project is supported through Australia Research Council Linkage grant LP150101172.

Appendix A. Supplementary data

Supplementary data related to this article can be found at <http://dx.doi.org/10.1016/j.ecss.2017.05.001>.

References

Batchelor, G.K., 1952. Diffusion in a field of homogeneous turbulence. In:

- Mathematical Proceedings of the Cambridge Philosophical Society, vol. 48. Cambridge Univ Press, pp. 345–362.
- Bendat, J.S., Piersol, A.G., 2011. Random Data: Analysis and Measurement Procedures, fourth ed., vol. 729. John Wiley & Sons, New Jersey.
- Brown, J., MacMaham, J., Reniers, A., Thornton, E., 2009. Surf zone diffusivity on a rip-channeled beach. *J. Geophys. Res. Ocean.* 114 (C11) <http://dx.doi.org/10.1029/2008JC005158> n/a-n/a.
- Chanson, H., Brown, R.J., Trevethan, M., 2012. Turbulence measurements in a small subtropical estuary under king tide conditions. *Environ. Fluid Mech.* 12 (3), 265–289. <http://dx.doi.org/10.1007/s10652-011-9234-z>.
- Fischer, H.B., List, E.J., Koh, R.C., Imberger, J., Brooks, N.H., 1979. *Mixing in Inland and Coastal Waters*. Academic Press, New York.
- Haza, A.C., Poje, A.C., Özgökmen, T.M., Martin, P., 2008. Relative dispersion from a high-resolution coastal model of the Adriatic Sea. *Ocean. Model.* 22 (1–2), 48–65. <http://dx.doi.org/10.1016/j.ocemod.2008.01.006>.
- Hey, R.D., Thorne, C.R., 1975. Secondary flows in river channels. *Area* 7 (3), 191–195. Retrieved from <http://www.jstor.org/stable/20001006>.
- Kalda, J., Soomere, T., Giudici, A., 2014. On the finite-time compressibility of the surface currents in the Gulf of Finland, the Baltic Sea. *J. Mar. Syst.* 129, 56–65. <http://dx.doi.org/10.1016/j.jmarsys.2012.08.010>.
- Kawanisi, K., 2004. Structure of turbulent flow in a shallow tidal estuary. *J. Hydraul. Eng.* 130 (4), 360–370. [http://dx.doi.org/10.1061/\(ASCE\)0733-9429\(2004\)130:4\(360\)](http://dx.doi.org/10.1061/(ASCE)0733-9429(2004)130:4(360)).
- Klein, P., Hua, B.L., 1990. The mesoscale variability of the sea surface temperature: an analytical and numerical model. *J. Mar. Res.* 48 (4), 729–763.
- Kolmogorov, A.N., 1941. Dissipation of energy in the locally isotropic turbulence. *Doklady Akad. Nauk SSSR* 32, 141 (English translation 1991). *Proc. Math. Phys. Sci.* 434 (1890), 15–17.
- LaCasce, J., 2008. Lagrangian statistics from oceanic and atmospheric observations. In: *Transport and Mixing in Geophysical Flows*. Springer, pp. 165–218.
- LaCasce, J., Bower, A., 2000. Relative dispersion in the subsurface North Atlantic. *J. Mar. Res.* 58 (6), 863–894. <http://dx.doi.org/10.1357/002224000763485737>.
- LaCasce, J.H., Ohlmann, C., 2003. Relative dispersion at the surface of the Gulf of Mexico. *J. Mar. Res.* 61 (3), 285–312. <http://dx.doi.org/10.1357/002224003322201205>.
- Legleiter, C.J., Kyriakidis, P.C., 2006. Forward and inverse transformations between Cartesian and channel-fitted coordinate systems for meandering rivers. *Math. Geol.* 38 (8), 927–958. <http://dx.doi.org/10.1007/s11004-006-9056-6>.
- List, E.J., Gartrel, G., Winant, C.D., 1990. Diffusion and dispersion in coastal waters. *J. Hydraul. Eng.* 116 (10), 1158–1179. [http://dx.doi.org/10.1061/\(ASCE\)0733-9429\(1990\)116:10\(1158\)](http://dx.doi.org/10.1061/(ASCE)0733-9429(1990)116:10(1158)).
- Manning, J.P., Churchill, J.H., 2006. Estimates of dispersion from clustered-drifter deployments on the southern flank of Georges Bank. *Deep Sea Res. Part II Top. Stud. Oceanogr.* 53 (23–24), 2501–2519. <http://dx.doi.org/10.1016/j.dsr2.2006.08.004>.
- Nezu, I., Nakagawa, H., 1993. *Turbulence in Open-channel Flows*. Paper presented at IAHR Monograph. IAHR Fluid Mechanics Section, Balkema, Rotterdam, The Netherlands.
- Obukhov, A.M., 1941. On the distribution of energy in the spectrum of turbulent flow. In: *Dokl. Akad. Nauk SSSR*, vol. 32, pp. 22–24.
- Okubo, A., Ebbesmeyer, C.C., 1976. Determination of vorticity, divergence, and deformation rates from analysis of drogoue observations. In: *Deep Sea Research and Oceanographic Abstracts*, vol. 23. Elsevier, pp. 349–352.
- Pinton, J.-F., Sawford, B.L., 2012. A Lagrangian view of turbulent dispersion and mixing. In: Davidson, P.A., Kaneda, Y., Sreenivasan, K.R. (Eds.), *Ten Chapters in Turbulence*. Cambridge University Press, New York.
- Poje, A.C., Özgökmen, T.M., Lipphardt, B.L., Haus, B.K., Ryan, E.H., Haza, A.C., et al., 2014. Submesoscale dispersion in the vicinity of the Deepwater Horizon spill. *Proc. Natl. Acad. Sci.* 111 (35), 12693–12698. <http://dx.doi.org/10.1073/pnas.1402452111>.
- Richardson, L.F., 1926. Atmospheric diffusion shown on a distance-neighbour graph. *Proc. R. Soc. Lond. Ser. A, Contain. Pap. a Math. Phys. Character* 110 (756), 709–737.
- Richez, C., 1998. The West Spitsbergen current as seen by SOFAR floats during the ARCTEMIZ 88 experiment: statistics, differential kinematic properties, and potential vorticity balance. *J. Geophys. Res. Ocean.* 103 (C8), 15539–15565. <http://dx.doi.org/10.1029/97JC02421>.
- Riddle, A., Lewis, R., 2000. Dispersion experiments in UK coastal waters. *Estuar. Coast. Shelf Sci.* 51 (2), 243–254. <http://dx.doi.org/10.1006/ecss.2000.0661>.
- Salazar, J.P., Collins, L.R., 2008. Two-particle dispersion in isotropic turbulent flows. *Annu. Rev. Fluid Mech.* 41 (1), 405–432. <http://dx.doi.org/10.1146/annurev.fluid.40.111406.102224>.
- Sawford, B., 2001. Turbulent relative dispersion. *Annu. Rev. Fluid Mech.* 33 (1), 289–317. <http://dx.doi.org/10.1146/annurev.fluid.33.1.289>.
- Schroeder, K., Chiggiato, J., Haza, A.C., Griffo, A., Özgökmen, T.M., Zanasca, P., et al., 2012. Targeted Lagrangian sampling of submesoscale dispersion at a coastal frontal zone. *Geophys. Res. Lett.* 39 (11), L11608. <http://dx.doi.org/10.1029/2012GL051879>.
- Situ, R., Brown, R.J., 2013. Mixing and dispersion of pollutants emitted from an outboard motor. *Mar. Pollut. Bull.* 69 (1–2), 19. <http://dx.doi.org/10.1016/j.marpolbul.2012.12.015>.
- Soomere, T., Viidebaum, M., Kalda, J., 2011. On dispersion properties of surface motions in the Gulf of Finland. *Proc. Est. Acad. Sci.* 60 (4), 269–279.
- Spydell, M.S., Feddersen, F., Olabarrieta, M., Chen, J., Guza, R.T., Raubenheimer, B., Elgar, S., 2015. Observed and modeled drifters at a tidal inlet. *J. Geophys. Res.*

- Ocean. 120 (7), 4825–4844. <http://dx.doi.org/10.1002/2014JC010541>.
- Stevens, C., 2010. Short-term dispersion and turbulence in a complex-shaped estuarine embayment. *Cont. Shelf Res.* 30 (5), 393–402. <http://dx.doi.org/10.1016/j.csr.2009.12.011>.
- Stocker, R., Imberger, J., 2003. Horizontal transport and dispersion in the surface layer of a medium-sized lake. *Limnol. Oceanogr.* 48 (3), 971–982. <http://dx.doi.org/10.4319/lo.2003.48.3.0971>.
- Suara, K., Ketterer, T., Fairweather, H., McCallum, A., Vanaki, S.M., Allan, C., Brown, R., 2016a. Cluster dispersion of low-cost GPS-tracked drifters in a shallow water. In: Proceedings of 10th Australasian Heat and Mass Transfer Conference. Australasian Fluid and Thermal Engineering Society.
- Suara, K.A., Brown, R.J., Borgas, M., 2016b. Eddy diffusivity: a single dispersion analysis of high resolution drifters in a tidal shallow estuary. *Environ. Fluid Mech.* 16 (5), 923–943. <http://dx.doi.org/10.1007/s10652-016-9458-z>.
- Suara, K.A., Brown, R.J., Chanson, H., 2015a. Turbulence and Mixing in the Environment: Multi-device Study in a Sub-tropical Estuary. Report No. CH99/15. Div. of Civil Engineering, The University of Queensland, Brisbane, Australia, ISBN 1742721389.
- Suara, K.A., Wang, C., Feng, Y., Brown, R.J., Chanson, H., Borgas, M., 2015b. High resolution GNSS-tracked drifter for studying surface dispersion in shallow water. *J. Atmos. Ocean. Technol.* 32 (3), 579–590. <http://dx.doi.org/10.1175/JTECH-D-14-00127.1>.
- Taylor, G.I., 1921. Diffusion by continuous movements. *Proc. Lond. Math. Soc.* 20, 196–211.
- Trevethan, M., 2008. A Fundamental Study of Turbulence and Turbulent Mixing in a Small Subtropical Estuary. Ph.D Thesis. School of Civil Engineering, The University of Queensland, Brisbane, Australia.
- Trevethan, M., Chanson, H., 2009. Turbulent mixing in a small estuary: detailed measurements. *Estuar. Coast. Shelf Sci.* 81 (2), 191–200. <http://dx.doi.org/10.1016/j.ecss.2008.10.020>.
- Trevethan, M., Chanson, H., Brown, R.J., 2008. Turbulent measurements in a small subtropical estuary with semidiurnal tides. *J. Hydraul. Eng.* 134 (11), 1665–1670. [http://dx.doi.org/10.1061/\(ASCE\)0733-9429\(2008\)134%3A11\(1665\)](http://dx.doi.org/10.1061/(ASCE)0733-9429(2008)134%3A11(1665)).
- Truesdell, C., 1954. The Kinematics of Vorticity. Indiana University Press, Bloomington.
- Tseng, R.S., 2002. On the dispersion and diffusion near estuaries and around Islands. *Estuar. Coast. Shelf Sci.* 54 (1), 89–100. <http://dx.doi.org/10.1006/ecss.2001.0830>.
- Whilden, K.A., Socolofsky, S.A., Chang, K.-A., Irish, J.L., 2014. Using surface drifter observations to measure tidal vortices and relative diffusion at Aransas Pass, Texas. *Environ. Fluid Mech.* 14 (5), 1147–1172. <http://dx.doi.org/10.1007/s10652-014-9361-4>.
- Zimmerman, J., 1986. The tidal whirlpool: a review of horizontal dispersion by tidal and residual currents. *Neth. J. Sea Res.* 20 (2), 133–154. [http://dx.doi.org/10.1016/0077-7579\(86\)90037-2](http://dx.doi.org/10.1016/0077-7579(86)90037-2).